PAPER

Testing the effects of body depth on fish maneuverability via robophysical models

Bioinspiration & Biomimetics

PAPER

Testing the effects of body depth on fish maneuverability via robophysical models

RECEIVED
22 June 2021

REVISED
25 October 2021

ACCEPTED FOR PUBLICATION
27 October 2021

PUBLISHED
29 November 2021

Stephen Howe*, Kelly Bryant, Andrew Duff and Henry Astley

University of Akron Ohio, United States of America
* Author to whom any correspondence should be addressed.

E-mail: Stephen.p.howe@outlook.com

Keywords: fish, maneuverability, comparative biomechanics, robophysical model

Supplementary material for this article is available online

Abstract

Fish show a wide diversity of body shapes which affect many aspects of their biology, including swimming and feeding performance, and defense from predators. Deep laterally compressed bodies are particularly common, and have evolved multiple times in different families. Functional hypotheses that explain these trends include predator defense and increased maneuverability. While there is strong evidence that increasing body depth helps fish avoid gape-limited predators, the evidence that body shape increases a fish's maneuverability is ambiguous. We used a two-pronged approach to explore the effects of body shape on the control of maneuvers using both live fish and a robotic model that allowed us to independently vary body shape. We captured ventral video of two tetra species (*Gymnocorymbus ternetzi* and *Aphyocharax anisitsi*) performing a wide range of maneuvers to confirm that both species of live fish utilize fundamentally similar body deformations to execute a turn, despite their different body depths. Both species use a propagating 'pulse' of midline curvature that is qualitatively similar to prior studies and displayed similar trends in the relationships between body kinematics and performance. We then tested the robotic model's maneuverability, defined as the total heading change and maximum centripetal acceleration generated during a single pulse, at a range of different input kinematics across three body shapes. We found that deepening bodies increase the robot's ability to change direction and centripetal acceleration, though centripetal acceleration exhibits diminishing returns beyond a certain body depth. By using a robotic model, we were able to isolate the effects of body shape on maneuverability and clarify this confounded relationship. Studying the functional morphology of complex traits such as body shape and their interaction with complex behavior like maneuverability benefits from both the broad view provided by comprehensive comparative studies, and the control of variables enabled by robophysical experiments.

1. Introduction

Bony fish are a diverse clade with a wide range of body shapes. The major axis of shape variation across many groups of fish is elongation vs body depth, where fish range from having long slender bodies to short deep bodies (Burns and Sidlauskas 2019; Claverie and Wainwright 2014; Price *et al* 2019). In water, there are high energetic penalties for straying from the most streamlined shapes. Fish that regularly swim in high flow or over long distances tend to be more fusiform and can have higher prolonged swimming speeds (critical swimming velocity), a metric that suggests greater swimming efficiency (Costa-Pereira *et al* 2016; Foster *et al* 2015; Franssen *et al* 2013; Haas *et al* 2015; Istead *et al* 2015; Moody and Lozano-Vilano 2018; Rubio-Gracia *et al* 2020; Svozil *et al* 2020; Yan *et al* 2013). Despite this selective pressure, fish that have short, deep bodies evolved multiple times across many different clades, both in fresh and salt-water fishes (Burns and Sidlauskas 2019; Claverie and Wainwright 2014; Feilich 2016; Fernando *et al* 2018; Price *et al* 2019).

There are two primary hypotheses to explain deep-bodied morphology in fish. First, deeper bodies evolved as a defense against gape-limited

predators (Brönmark and Miner 1992; Nilsson *et al* 1995; Wahl and Stein 1988). Changes in body shape can be plastically induced in crucian carp by the presence of predators (Brönmark and Miner 1992). Predatory fish have increased handling time when eating deeper-bodied fish and prefer more fusiform foods (Nilsson *et al* 1995; Wahl and Stein 1988). Second, deep bodies are also hypothesized to affect maneuverability (Domenici *et al* 2008; Langerhans 2009; Moody and Lozano-Vilano 2018; Webb 1983). When comparing turning performance between trout and smallmouth bass, Webb (1983) found that bass could achieve tighter turn radii than trout, and attributed this difference to increased turning forces available to the bass due to increased added mass and lateral projected area. Juvenile bluegill have increased body depths relative to their earlier and later growth stages and have higher accelerations and displacements in escape turns relative to body size (Gerry *et al* 2016). Crucian carp with phenotypically plastic predator-induced increased body depth show increased speed, acceleration, and turning rate (Domenici *et al* 2008). Intraspecific differences in body flexibility and the shape of the caudal region have highlighted tradeoffs between predator avoidance and economical swimming (Langerhans 2009; Moody and Lozano-Vilano 2018). In some cases, predation pressure appears to supersede economical swimming, with prey fish exhibiting morphologies optimized for unsteady swimming, despite living in waters with high flow rates, which would normally select for fusiform body shapes (Moody and Lozano-Vilano 2018).

The biomechanical relationship between body shape and maneuverability is not fully understood. Early work by Webb (1983) proposed the relationship between body depth and minimum turn radius, and several later papers suggest that deeper bodies are also associated with increased turn velocity and acceleration (Domenici *et al* 2008; Gerry *et al* 2016). However, other papers contradict this hypothesis (Schrank *et al* 1999; Webb 1978). Webb (1978) found that the differences in fast start displacement, velocity, and acceleration were better explained by percent muscle mass in fish than their body depth. Schrank *et al* (1999) found that the fusiform goldfish completed turns faster than the deeper-bodied silver dollar and angelfish. However, in this experiment, the fish were made to turn in confined raceways rather than open water, which may give an advantage to the goldfish, as the walls could have limited the angelfish's use of its pectoral fins (Schrank *et al* 1999).

The function of morphology can be difficult to understand with live organisms because there are many correlated variables that are impossible to control (Garland and Adolph 1994). Differences in muscle physiology, muscle architecture, and behavior can vary widely between species (Astley 2016). Phylogeny is another confounding factor that if not handled properly can lead to improper conclusions being drawn based on faulty statistical assumptions (Felsenstein 1985). Because of these confounding issues, it is difficult to draw conclusions based on two species comparisons (Garland and Adolph 1994). An observed performance difference may be due to uncontrolled factors rather than the trait of interest. Similarly, not observing a performance difference between species may be due to compensation via another mechanism that was not controlled. Body shape is a composite feature that affects and is affected by several different selective pressures. A comparative approach to understand how body shape interacts with turning would require experimental data from a wide range of fishes, including the performance data, the hypothesized morphological correlates, and as many potential confounding factors as possible, all while explicitly accounting for phylogenetic effects (Garland and Adolph 1994).

Robotics can provide a powerful alternative to comparative studies for the elucidation of form/function relationships. Robots dramatically reduce variability within a system, isolating the effects of a feature of interest (Feilich and Lauder 2015; Shelton *et al* 2014; Tangorra *et al* 2010; Wolf *et al* 2020). Robophysical models simplify a system by isolating certain traits, or aspects of traits that would otherwise be confounded by evolutionary history, or interactions with other traits (Lauder 1996). Robophysical models are useful in systems where the physics of the system are complex and or difficult to simulate, as is the case with granular media (Aguilar *et al* 2016). In swimming systems, robots can be used instead of fluid simulations, which are complex and computationally expensive. Decoupling shape and behavior allows for experiments that examine the interactions between traits which are normally tightly correlated, like body shape and swimming kinematics (Borazjani and Sotiropoulos 2010).

While differences in maneuverability are usually compared among body shapes during high-intensity maneuvers (Domenici *et al* 2008; Gerry *et al* 2016; Webb 1983), Webb (1983) suggests that the minimum turning radius is smaller in deeper-bodied fish, regardless of velocity. Routine turns, which are slower than escape responses (Howe and Astley 2020), make up a large portion of a fish's locomotion repertoire but are seldom studied in detail. We expect that deeper bodies will show higher performance (increased heading change and centripetal acceleration) for the same body curvature and turn duration (Webb 1983).

We first used two species of similarly sized fish (*Gymnocorymbus ternetzi* and *Aphyocharax anisitsi*) that have different body depths to explore the control relationships between kinematics and performance in voluntary maneuvers to ensure that deep- and shallow-bodied fish turned via similar mechanisms. Two species comparisons can be limited in their

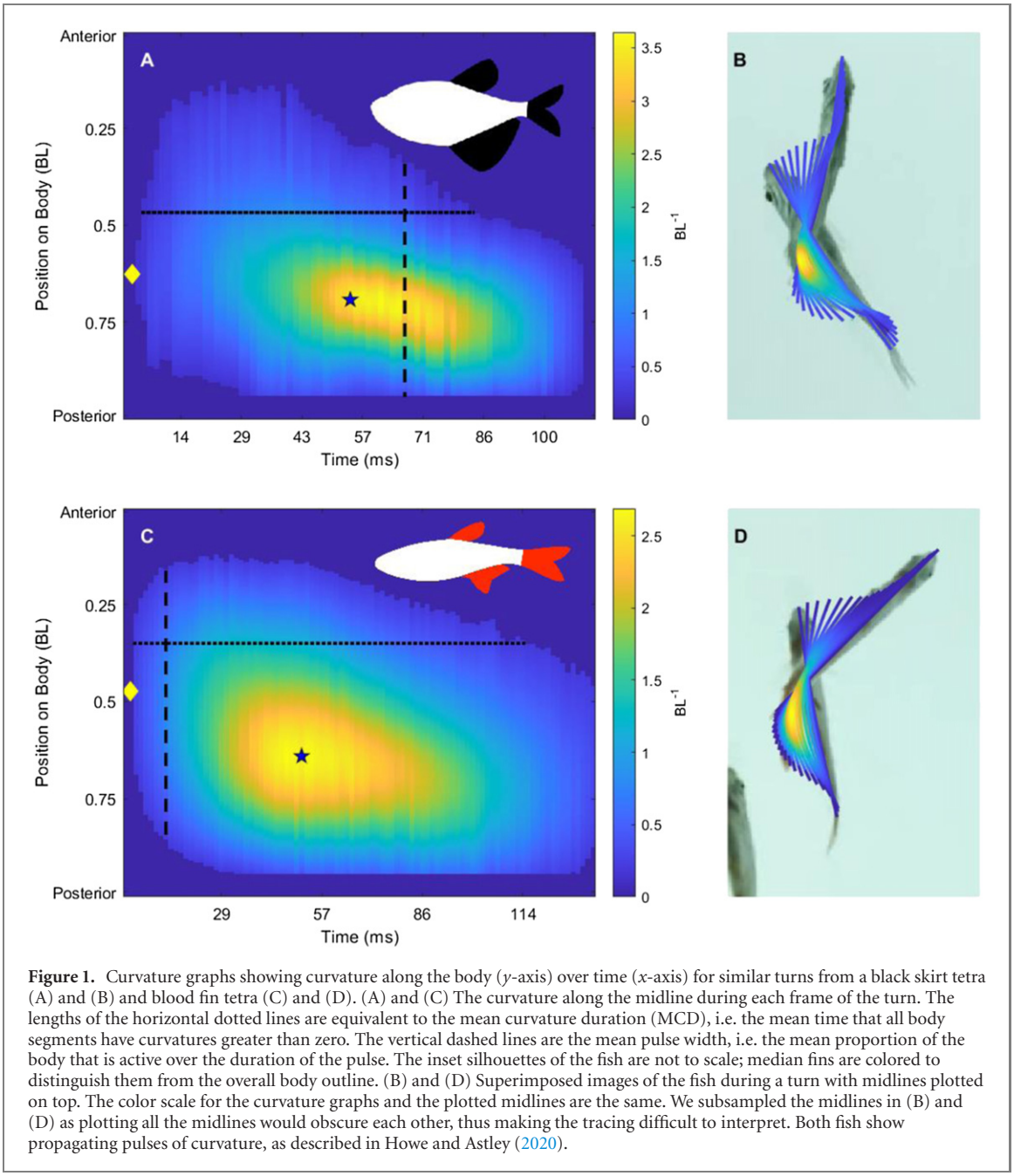

Figure 1. Curvature graphs showing curvature along the body (*y*-axis) over time (*x*-axis) for similar turns from a black skirt tetra (A) and (B) and blood fin tetra (C) and (D). (A) and (C) The curvature along the midline during each frame of the turn. The lengths of the horizontal dotted lines are equivalent to the mean curvature duration (MCD), i.e. the mean time that all body segments have curvatures greater than zero. The vertical dashed lines are the mean pulse width, i.e. the mean proportion of the body that is active over the duration of the pulse. The inset silhouettes of the fish are not to scale; median fins are colored to distinguish them from the overall body outline. (B) and (D) Superimposed images of the fish during a turn with midlines plotted on top. The color scale for the curvature graphs and the plotted midlines are the same. We subsampled the midlines in (B) and (D) as plotting all the midlines would obscure each other, thus making the tracing difficult to interpret. Both fish show propagating pulses of curvature, as described in Howe and Astley (2020).

usefulness when studying functional morphology (Garland and Adolph 1994), but the data we gather from live fish provide a baseline to compare to the results from the robotic model and validate the robotic control scheme. To directly test the relationships between body depth and turn performance, we used a robotic model that allowed us to change only the body depth of the model, holding all other variables constant, while moving through a bio-inspired control scheme (Howe *et al* 2021).

2. Methods

2.1. Live fish experiments

We used two different species of characin of different body depth: eight blood fin tetras (*A. anisitsi*, Eigenmann and Kennedy 1903) (mean ± s.d.: body length: 24.2 ± 1.4 mm, body depth: 5.6 ± 0.5 mm, depth:length ratio: 0.23 ± 0.01) (figure 1(A) inset), and eight black skirt tetras (*G. ternetzi*, Boulenger 1895) (mean ± s.d.: body length: 30 ± 1.8 mm, body depth: 14.3 ± 1.4 mm, depth:length ratio: 0.49 ± 0.02) (figure 1(B) inset). The two species had significantly different depth:length ratios (DF 14, *T* ratio: 28.04, $p < 0.0001$). All individuals were housed in a community tank with only conspecifics. To achieve normal behavior, we had to swim groups of three or four fish, as lone fish exhibited aberrant 'anxious' behavior. We conducted trials from each group of fish over the course of the day. At the end of the day, the fish in the group were euthanized so they could not be accidentally re-sampled. We simultaneously recorded

video from two orthogonal horizontal angles. During digitization these views allowed us to reliably identify individual fish using size and distinctive markings. All live fish experiments were approved under the University of Akron IACUC protocol #17-02-03-AFC.

We collected video of routine turns, which is spontaneous turning behavior that is recorded opportunistically. Trials were run in a 30 cm × 30 cm × 25 cm (L × W × H) acrylic tank. The fish swam in still water at the same temperature the fish were housed (23° Celsius). The water was periodically reoxygenated with a bubbler, approximately every 20 videos collected. The bubbler was removed during filming as the bubbles interfered with the image analysis. Ventral videos were filmed using an Edgertronic® SC1 color high-speed video camera (Sanstreak Corp. San Jose, CA, USA) via a 45° mirror placed below the tank. The videos were lit with LED light tables (Porta-Trace 1824 LED lightbox, Gagne Inc., Johnson City NY) on two sides and from above, backlighting the fish. All videos were recorded at 700 frames per second with a shutter speed of 1/1000th second.

The videos were analyzed using a custom MATLAB code detailed in (Howe and Astley 2020) and are included in the data dryad repository linked at the end of the manuscript. To summarize, the experimenter identifies the subject fish in the first frame of the video. The code then tracks the individual fish over the course of the video. For each frame, the image of the fish was converted to grayscale and the edges of the fish are found using a gradient filter. The silhouette of the fish was binarized by filling in the edges identified in the gradient filter. The binarized image was then skeletonized and de-spurred if necessary. The skeletonization process shortens the midline of the fish, and so a subroutine re-extends the midline to the edges of the binarized image. After extension, the midline points were then smoothed using a cubic spline and then interpolated to a fixed number of points. Curvature (the inverse of the radius of curvature) was calculated at each point along the midline by fitting a circle to three points: two points 7% the length of the midline anterior and posterior to the target point, and the target point itself and normalized by midline length. The curvature values for each frame were captured in a matrix that holds all the curvature values for the duration of the video.

When the curvature values along the body are mapped over the duration of the turn, a region of posteriorly propagating curvature becomes clear (termed a 'pulse') (figures 1(A) and (C)) (Howe and Astley 2020). To limit curvature noise, we used a threshold of 0.2 BL^{-1} to isolate pulses from the background. In our prior paper describing routine maneuvers, we measured a wide range of variables that describe different aspects of the body deformations during the turn, but found that a reduced set of four variables accounted for a majority of the variation (Howe and Astley 2020), which we used for analysis of this data set: maximum overall curvature (MOC), mean curvature duration MCD, mean pulse width, and pulse origin. MOC is calculated by determining the mean curvature of the midline for every frame during the pulse, including regions of low or zero curvature to account for the length of the body that is engaged in the pulse, and selecting the maximum of these values. MOC values are reported as the inverse of body length. MCD is the mean duration that each point along the midline is above the curvature threshold and is reported in milliseconds (ms) for live fish. Mean pulse width is the average proportion of the midline that is above the curvature threshold over the duration of the turn, which is a metric of how much of the body is engaged over the duration of the pulse. Pulse origin is the point on the body that corresponds to the maximum curvature of the first frame where the midline achieves a curvature greater than the threshold. Pulse origin and mean width are reported as percentage of body length.

In our prior work, we found that two turn outcome variables, total heading change and maximum centripetal acceleration, explained a large portion of the variability in describing the whole-body turn performance (Howe and Astley 2020). The heading of the fish is calculated using the first point on the midline and a point 15% of the length of the midline from the head. This distance approximates the length of the cranium in our fish and is effectively rigid. The change in heading was calculated between frames by finding the angle between the lines created by the rostral and cranial points on the midlines of the two frames. These instantaneous heading changes are summed over the course of the turn to calculate the total heading change for the pulse. We also calculated recoil: the difference between the maximum heading change the fish achieves minus the final trajectory when the fish straightens. We tracked the centroid of the ventral binary image of the fish as an approximation of the center of mass. There are several methods to approximate or calculate the center of mass of a fish in video (Fleuren *et al* 2018; Jayne and Lauder 1993; Webb, 1983; Westneat *et al* 1998); our method of tracking the centroid largely agrees with these prior methods (Howe and Astley 2020). The path of the centroid is smoothed over the duration of the video using a cubic spline, and those smoothed values are used to calculate velocity and acceleration. Linear acceleration is the component of acceleration that is parallel to the velocity vector at a given time. Centripetal acceleration is the component of acceleration that is perpendicular to the velocity vector at a given time. We report the mean linear acceleration for the entire pulse and the maximum instantaneous centripetal acceleration in m sec^{-2}.

After digitizing the videos, we found that several fish did not produce enough turns to be included in the analysis. We ultimately included 15 turns from five individuals from each species for a total of 150 turns.

If an individual produced more than 15 turns we randomly selected 15 turns for that individual using the random subset tool available in JMP 16.

2.2. Robot experiments

The robotic fish was based around an actuated backbone that was used previously (Howe *et al* 2021), and was comprised of five waterproof servos (Hitec HS-5086WP, max torque: 0.3 N m stall current draw 1800 mA) that were connected using custom 3D printed brackets. We 3D printed body shells to attach to the backbone, creating three robots with different body shapes that captured a range of body depths (figure 2). All 3D parts were designed in Autodesk Fusion 360 (Autodesk Inc., San Francisco, California). The body shape was generalized and symmetrical across the midsagittal and frontal planes. All body shape parameters are ultimately rooted in the length of the robot (0.46 m). The lateral profile was set by symmetrical splines that had anchor points at the head, height at midbody, and the tail. The angle of the spline fit at the head was set relative to the body depth ($2\tan^{-1}(\text{Depth}\cdot\text{Length}^{-1})$). The spline fit at the tail was fixed horizontally. The spline fit at the maximum depth was left unconstrained. Because the midbody anchor point was unconstrained the maximum depth occurred slightly ahead or behind the midpoint (shallow depth 53%, medium depth 38% BL, deep body 42% BL), but was minimally different from the depth at midbody. The shallow body shape depth at midbody was 20% the total length, the medium shape was 38.5% the total length, and the deep shape was 57% the total length, encompassing the range of variation seen in the live fish species in this experiment. The same procedure was used for the splines that defined the width of the robot, with anchor points at the head, midbody, and tail. The width was set to 20% of the total length for all shapes and was limited by the width of the motorized backbone. The body was split into six sections: the head, four body segments, and the peduncle. The body length was determined by the number of motors used and the height of the motors that needed to be encased. Each motor had a maximum excursion of $\pm 45°$, which was accommodated by cutting wedges out of either side of the 3D designed body, centered around each motor axis. All the body shells were printed out of Polylactic acid (PLA) filament with no internal voids. The brackets were printed out of Acrylonitrile butadiene styrene (ABS) filament with no internal voids. Stereolithography files for all 3D printed components are available in the data dryad repository linked at the end of the manuscript. We hand sewed Lycra skins for each body shape to reduce water circulation between the segments, which improved performance in our prior paper (Howe *et al* 2021). We constructed the tail from two 0.5 mm sheets of Mylar anchored within the caudal peduncle with bolts. The tail shape remained the same across all body shape tests to prevent confounding variation. Closed cell foam was used for buoyancy and stainless-steel nuts and bolts were used as ballast. To fine tune buoyancy, we constructed an adjustable buoyancy control device using latex tubing, a large polypropylene syringe, and a balloon. The syringe contained and protected the balloon in the robot body; air was manually added or removed from the balloon through the tubing and then sealed off.

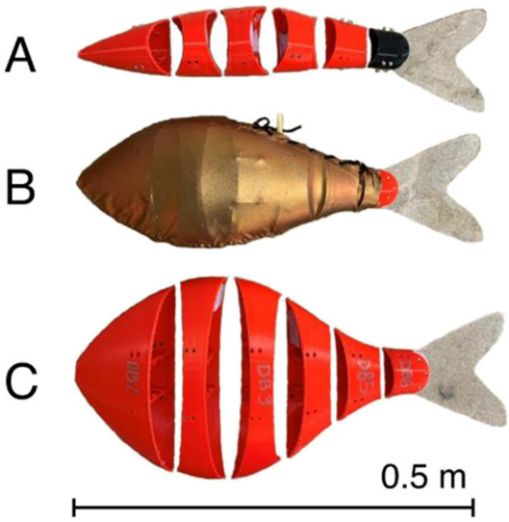

Figure 2. Body shells for each robot shape: (A) shallow, (B) medium, (C) deep. The medium shape shows the fully assembled robot with tailored skin.

The motors were controlled using an Arduino Uno microprocessor (Arduino, Turin, Italy) and powered by a Mastech HY-3020E DC power supply. The voltage of the power supply was set to six volts, the maximum voltage rating for the motors, and the allowed amperage was unlimited. One aspect we were not able to measure was applied motor torque. All the motors were supplied with the same voltage and given the same input commands but were required to execute those commands on different body shapes. The forces required to deflect the deeper body would be higher, placing more load on the motors. We found that the motor position errors did not change, regardless of the turn intensity within body shape, which indicates the error we observed was due to other factors. We would expect that the deep body shape would be unable to execute fast high-angle turns if motor torque was insufficient, however this was not the case.

The algorithm used to control the kinematics of the robot was drawn from the bio-inspired algorithm developed in our previous paper (Howe *et al* 2021) (figure 3) and based on kinematics observed in giant danios. This swimming algorithm consists of bending pulses that are defined by input amplitude, duration, and origin (figure 3); however, origin was not varied in these tests, as it differed only minimally between species. These pulses can be strung together to reconstruct steady swimming while allowing for the integration of turns and other behavior. We looked at

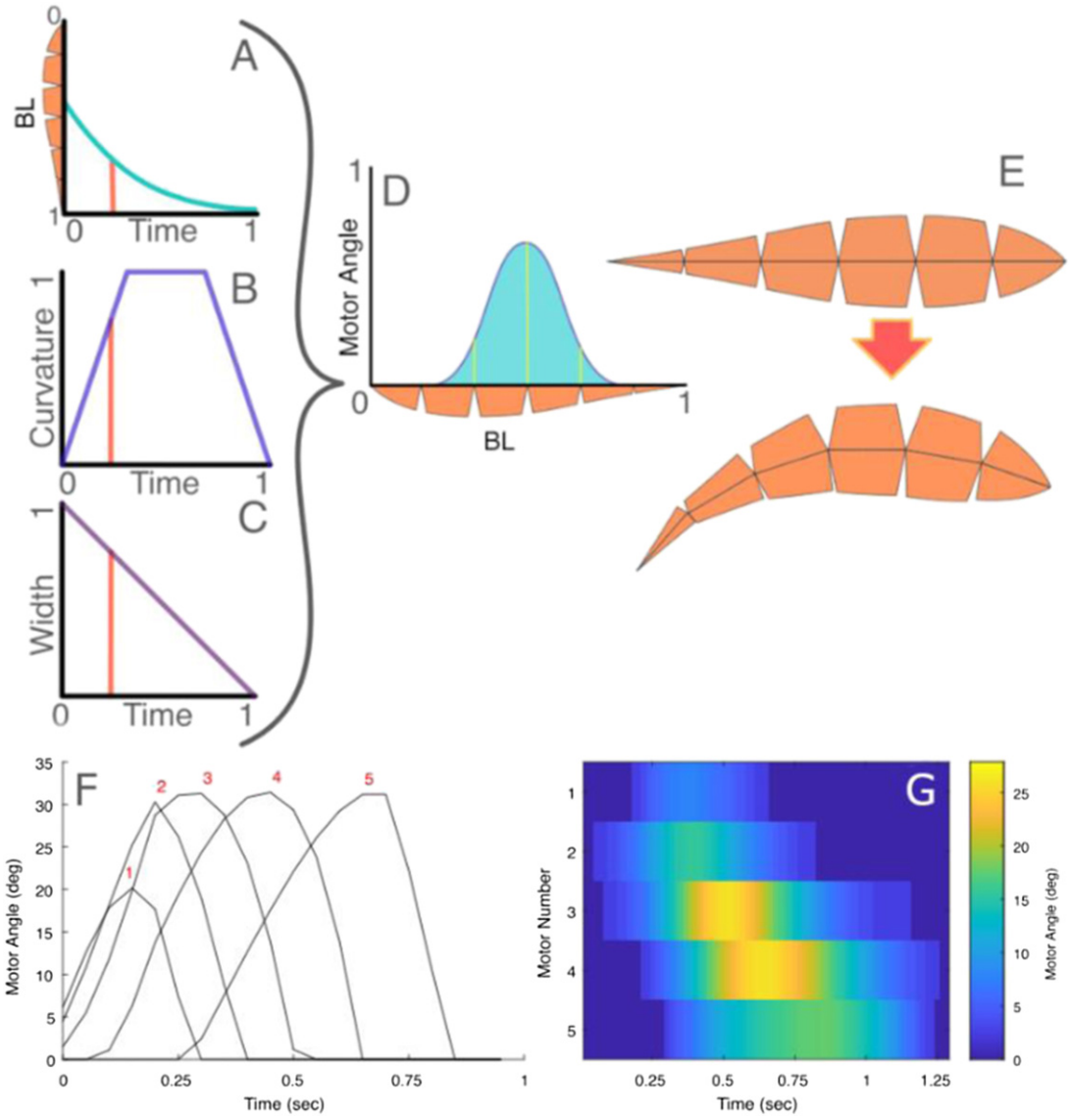

Figure 3. Control of the robophysical model. (A)–(E) A schematic of the algorithm that controls the pulse. (A)–(C) Transform functions defining the position of the bending peak, the amplitude, and the width. (D) The sinusoidal peak fitted to the maximum amplitude and width boundaries derived from (A)–(C). (E) An example of the body conformation change after the motors receive instructions. (F) The commanded angles calculated from the pulse algorithm over the duration of the turn. (G) The heat map showing the measured angles from the medium-depth body shape robot executing the commanded angles from (F). Reproduced from (Howe *et al*).

single pulse turns across a range of input angles and durations. Each test run consisted of three full tail beats, a short glide, the turn, and another glide. The forward swimming phase allowed the robot to enter the turn with a positive initial velocity. The glide phase on either side of the turn ensured the robot started and ended the turn with a straight posture.

We tested maximum motor angles of 18°, 24.75°, 31.5°, 38.25°, and 45°, and turn durations of 0.5, 1.0, 1.5, 2.0, and 2.5 seconds. We did not sample the entire angle duration combination matrix (table S1 (https://stacks.iop.org/BB/17/016002/mmedia)). We sampled every duration combination with a maximum motor angle 31.5°, every angle combination with a turn duration of 1.5 sec, and the diagonals of the matrix. We collected five videos from each angle/duration combination for each body shape: 85 videos per shape, 255 videos in total. Ventral view videos were collected using a GoPro Hero 6 (GoPro, San Mateo, California), filmed at 60 frames per second 1080p using the linear view setting (movie 1). We collected videos in the Ocasek Natatorium on the University of Akron campus (Akron, Ohio). The camera was set on a tripod about 2.5 meters below the water surface, giving us a field of view of approximately 3.5 × 5 meters. One experimenter positioned the robot at the beginning of each trial, and another maneuvered the servo wires that were attached to a PVC pipe to avoid pull or drag on the robot. The robot was neutrally buoyant and free swimming, and we maneuvered the wires without altering the course or speed of the robot.

Videos were processed using a modified version of the code described in the live fish section, which

was used in Howe and Astley (2020) and Howe *et al* (2021). Instead of reporting midline curvature, as in the live fish, we approximated the joint centers based on the body length in the video and the known positions of the motors as a proportion of body length. We used these data to calculate the joint angles. We measured the maximum summed motor angle and turn duration as the realized kinematics of the commanded kinematic inputs. To find the maximum summed motor angle, we added the motor angles together during each frame of the video and recorded the maximum of those sums. Turn duration is the duration that a motor is above the angle threshold of 5%. We calculated the summed motor angle error and duration error as the difference between the measured variable and the commanded variable divided by the commanded variable. Like the live fish, we track the heading and centroid of the robot. We report the total heading change, recoil, mean linear acceleration, and maximum centripetal acceleration, as in the fish. Recoil is the difference between the maximum heading change the robot achieves and the final heading change the robot achieves when the body straightens. Mean linear acceleration is the average of all the linear acceleration values over the duration of the turn. Having measured the linear and centripetal accelerations for each body shape, we used an estimation of the mass of each robot to estimate the linear and centripetal forces generated by each body shape. Because our robots have skins, they accelerate both the hardware that defines their body shape and drives motion as well as the water contained within the volume of the body. We assumed that each robot had the density of water and found the volume of each body envelope to estimate mass. We could then multiply mass by acceleration to estimate force. We did not log normalize any of the variables from the robot data set as it did not significantly change the behavior of the model and complicated interpretation.

3. Statistics

3.1. Live fish

The purpose of the statistical tests on the live fish were to establish similarity in kinematics and control between species. Because we only have two species, we cannot effectively evaluate differences in maneuverability performance with these tests. To compare the mean values for our midline shape variables (maximum overall curvature (MOC), mean curvature duration (MCD), pulse origin, and pulse width), we used a nested ANOVA, where species was the main effect with individual nested within species. These tests were run using the standard least squares personality using the restricted maximum likelihood method with unbounded variance components. The variance components for individual can be found in table S1.

To explore the relationship between midline shape, change, and turn performance, we constructed a linear mixed model using the fixed effects of species, MOC, MCD, and the full set of interaction terms. We included individual as a random effect nested within species. This base model was separately fitted to the total heading change, recoil, mean linear acceleration, and maximum centripetal acceleration. The acceleration values were significantly skewed and thus log normalized before including them in the linear model. For linear acceleration, we had several turns that had negative mean accelerations (blood fin $n = 5$, black skirt $n = 12$) (i.e. the fish decelerated on average). As these negative values could not be log transformed alongside the positive values, and because the total number of turns was small and spread across multiple individuals, we elected to exclude them from the model. Log transforming values between one and zero results in negative numbers that proceed toward negative infinity as the value approaches zero. This can cause the appearance of outliers as fish execute turns that have accelerations that approach zero. To correct for this, we added 1 to ensure all the acceleration values were greater than 1. The total number of turns analyzed in the linear acceleration model was 133. The variance components for individual can be found in table S1. We log transformed the mean active duration as well as the acceleration variables due to data skew. We did not log transform the MOC and total heading change to ease interpretation; we ran separate models with these data logged as well and it did not significantly change the behavior of the models.

3.2. Robots

Because we did not collect the full angle/duration combination matrix, as well as due to variation in achieved kinematics, we were unable to do a full-factorial three-way ANOVA. Instead, we treated the input angles and durations as continuous factors and created linear models with body shape, input duration, input angle, and the full set of interaction terms as fixed effects. This model was fitted to the summed angle error and duration error response terms. The angle error was positive across all body shapes (table 3). The duration error was the highest in the medium-depth body shape (table 3). Because there was significant error in the motor kinematics, we used the measured motor kinematics to create models to test their effects on whole body outcomes; the model consisted of body shape, measured summed motor angle, measured turn duration, and the full set of interactions as fixed effects. This model was fitted separately to the outcome variables: total heading change, recoil, mean linear acceleration, maximum centripetal acceleration, mean linear force, and maximum centripetal force.

All statistical models were conducted in JMP 16 (SAS Institute Inc., Independence OH, USA), and

Table 1. Marginal means of the midline curvature kinematics and turn performance outcomes in the live fish. The estimates for midline kinematics are the means for each species. The estimates for the turn performance outcomes are the estimated means for each species from the model that includes the effects of MOC and MCD. The degrees of freedom for the midline kinematic variables are derived from the sample size and number of tests. The degrees of freedom for the turn performance outcomes are estimated from the mixed model.

		N	SPECIES	MEAN	STD ERROR	PAIRWISE	DF
MIDLINE KINEMATIC VARIABLES	Maximum Overall Curvature (BL^{-1})	150	SHALLOW	1.22	0.09	A	1,8
			DEEP	0.90	0.09	B	1,8
	Mean Curvature Duration (ms)	150	SHALLOW	113.27	15.64	A	1,8
			DEEP	125.88	15.64	A	1,8
	Pulse Origin (BL)	150	SHALLOW	0.483	0.011	A	1,8
			DEEP	0.552	0.011	B	1,8
	Mean Pulse Width (BL)	150	SHALLOW	0.70	0.01	A	1,8
			DEEP	0.59	0.01	B	1,8
TURN PERFORMANCE OUTCOMES	Total Heading Change (Deg)	150	SHALLOW	35.26	3.47	A	7.62
			DEEP	55.53	3.56	B	8.44
	Recoil (Deg)	150	SHALLOW	1.96	0.27	A	9.75
			DEEP	1.09	0.31	A	16.35
	Positive Mean Linear Acceleration Log ($BL{\cdot}S^{-2}+1$)	133	SHALLOW	1.92	0.09	A	7.14
			DEEP	2.94	0.11	B	16.84
	Maximum Centripetal Acceleration Log ($BL{\cdot}S^{-2}$)	150	SHALLOW	2.72	0.15	A	7.61
			DEEP	3.38	0.16	B	8.91

Table 2. Parameter estimates and effect tests for significant terms in the live fish linear models. The intercept test statistic is a *T* ratio instead of an *F* ratio. The degrees of freedom are estimated by the model. The full table of parameter estimates and fixed effect tests can be found in the supplementary materials.

	SOURCE		ESTIMATE	STD ERR	DF	F-RATIO	P > F
TOTAL HEADING CHANGE	N=150	Intercept	-58.98	10.39	139.6	T=-5.68	<.0001
	Species		-10.14	2.49	8	16.61	0.0035
	Maximum Overall Curvature (MOC)		44.89	2.35	136.5	363.86	<.0001
	Species*MOC		-10.03	2.35	136.5	18.16	<.0001
	Log[Mean Curvature Duration (MCD)]		12.18	2.28	139.1	28.62	<.0001
POSITIVE MEAN LINEAR ACCELERATION	N=133	Intercept	11.92	0.72	89.6	T=16.59	<.0001
	Species		-0.51	0.07	11.6	53.69	<.0001
	Maximum Overall Curvature (MOC)		1.73	0.18	122	96.86	<.0001
	Log[Mean Curvature Duration (MCD)]		-0.45	0.18	122	6.51	0.012
	MOC*Log[MCD]		-2.46	0.17	108.1	220.23	<.0001
MAXIMUM CENTRIPETAL ACCELERATION	N=150	Intercept	6.10	0.57	139.9	T=10.79	<.0001
	Species		-0.33	0.11	8.2	8.92	0.02
	Maximum Overall Curvature (MOC)		1.42	0.13	137.9	119.95	<.0001
	Log[Mean Curvature Duration (MCD)]		-0.98	0.13	141	61.14	<.0001
	MOC*Log[MCD]		-0.55	0.21	139.1	7.17	0.008

were significant after Bonferroni correction (see table S2 for ANOVA).

The full models for the live fish experiments can be viewed in table S1, the full models for the robot experiments can be viewed in table S2, and the full data sets for the live fish and robot experiments can be viewed in tables S3 and S4, respectively. The raw data, including source videos, can be accessed in the data dryad repository linked at the end of the manuscript.

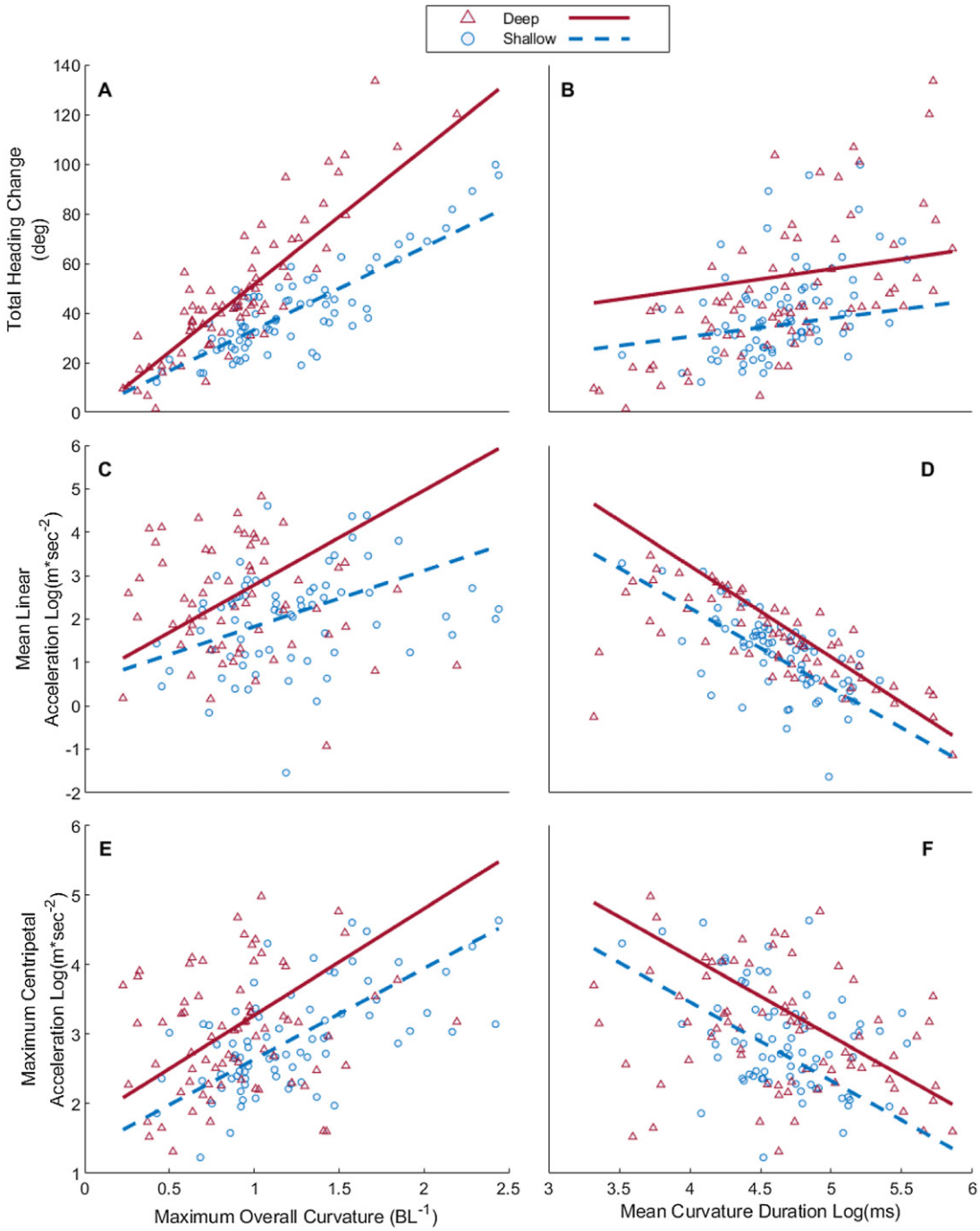

Figure 4. The linear model of live fish maneuver performance space. The lines plotted show the interaction between body deformation variables and species.

4. Results

4.1. Live fish

We observed 15 routine turns for five individuals in both black skirt and blood fin tetras for a total of 75 turns per species and 150 total (133 in the linear mixed model for linear acceleration). Across those turns they achieved MOC values ranging from 0.22 to 2.44 BL^{-1} (mean ± s.d.: 1.06 ± 0.44). The MCD ranged from 27.7 ms to 350.7 ms (mean ± s.d.: 119.6 ± 63.4). The total heading change ranged from 1° to 134° (mean ± s.d.: 44 ± 23). Maximum centripetal acceleration had a range of 3 BL sec^{-2} to 146 BL sec^{-2} (mean ± s.d.: 27 ± 25). Mean linear acceleration had a range of −31 BL sec^{-2} to 124 BL sec^{-2} (mean ± s.d.: 15 ± 22). Comparisons of estimated means within species can be found in table 1.

All the linear models showed the same basic relationships between species. Both MOC and MCD had significant positive effects on the total heading change (table 2, figures 4(A) and (B)). The MOC had significant positive effects on positive mean linear acceleration and maximum centripetal acceleration, (table 2, figures 4(C) and (E)). The MCD

Table 3. The marginal means of motor performance and turn outcomes in the robotic models. The degrees of freedom for the model were Num/Den: 11/243.

	BODY DEPTH	MARGINAL MEAN	STD ERROR	PAIRWISE
SUMMED ANGLE ERROR (%)	Deep	0.29	0.02	A
	Medium	0.31	0.02	A
	Shallow	0.26	0.02	A
TURN DURATION ERROR (%)	Deep	0.003	0.02	A
	Medium	0.16	0.02	B
	Shallow	-0.07	0.02	A
TOTAL HEADING CHANGE (DEG)	Deep	34.04	0.61	A
	Medium	36.69	0.62	B
	Shallow	17.74	0.59	C
RECOIL (DEG)	Deep	3.45	0.39	A
	Medium	6.92	0.40	B
	Shallow	22.46	0.38	C
MEAN LINEAR ACCELERATION (BL·SEC^{-2})	Deep	0.015	0.007	A
	Medium	0.024	0.008	AB
	Shallow	0.048	0.007	B
MAXIMUM CENTRIPETAL ACCELERATION (BL·SEC^{-2})	Deep	0.42	0.01	A
	Medium	0.55	0.01	B
	Shallow	0.23	0.01	C
MEAN LINEAR FORCE(N)	Deep	0.03	0.01	A
	Medium	0.03	0.01	A
	Shallow	0.09	0.01	B
MAXIMUM CENTRIPETAL FORCE (N)	Deep	0.83	0.02	A
	Medium	0.76	0.02	B
	Shallow	0.46	0.02	C

had significant negative effects on positive mean linear acceleration and maximum centripetal acceleration, i.e. shorter turn durations had higher accelerations (table 2, figures 4(D) and (F)). Species was a significant effect in the heading change, positive linear acceleration, and centripetal acceleration models, with deep-bodied fish having higher accelerations and heading changes than shallow-bodied fish (table 2, figure 4). The MOC and mean active duration had inverse effects on negative linear acceleration when compared to positive linear acceleration; increasing maximum average curvature and shorter turn durations resulted in greater deceleration (table 2, figures 4(C) and (D)).

4.2. Robot

Despite quantitative differences between the species examined in this study, the overall relationships between midline kinematics and turn performance outcomes are similar between these species and the giant danio examined in Howe and Astley (2020). As the robot algorithm developed in Howe *et al* (2021) was based on those giant danio data it follows that use of the same algorithm is appropriate to control the different robot shapes in this study.

The robot completed turns across all body shapes and input parameters with a measured maximum summed motor angle that ranged from 34° to 114° (mean ± s.d.: 70 ± 19°) (movie 1). The measured pulse duration ranged from 0.5 sec to 3.3 sec (mean ± s.d.: 1.5 ± 0.6 sec). The total heading change ranged from 1° to 71° (mean ± s.d.: 30 ± 15°). Recoil ranged from 0° to 41° (mean ± s.d.: 11 ± 10°). Mean linear acceleration ranged from −0.04 BL sec^{-2} to 0.25 BL sec^{-2} (mean ± s.d.: 0.02 ± 0.05 BL sec^{-2}). The shallow body depth had several turns that showed high mean linear acceleration, but we could not find any indication that these values were the result of an error. Maximum centripetal acceleration ranged from 0.01 BL sec^{-2} to 0.49 m sec^{-2} (mean ± s.d.: 0.18 ± 0.1 BL sec^{-2}). Maximum centripetal force ranged from 0.5N to 1.72N (mean ± s.d.: 0.68 ± 0.35N). The means and pairwise comparisons between body shapes can be found in table 3.

The medium-depth body shape had the highest total heading changes over the deep body shape by a

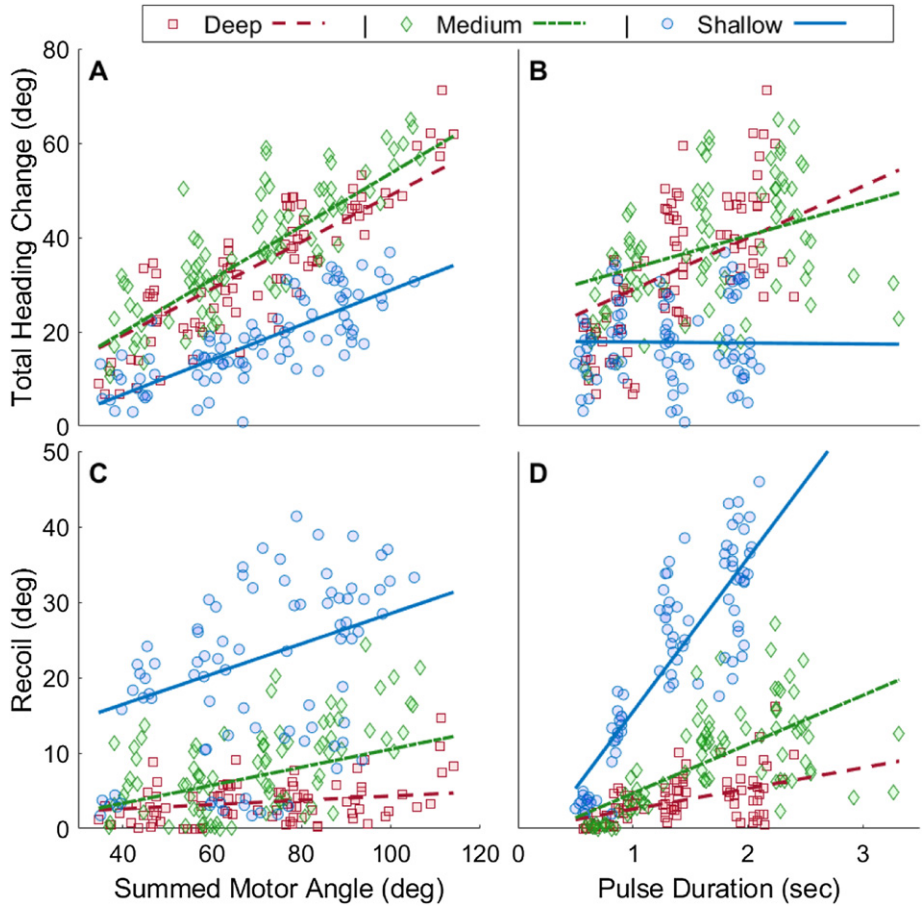

Figure 5. Linear models between measured motor kinematics and heading change variables in the three robotic models. Panes (A) and (B) show the relationships between the measured control variables and total heading change. Panes (C) and (D) show the relationships between the measured motor control variables and recoil.

small but significant margin. Both deeper body shapes had significantly higher total heading changes than the shallow body shape. The summed motor angle had a significant positive effect on the total heading change across all body shapes (figure 5). The slope of the interaction between the summed motor angle and total heading change in the medium-depth body shape was significantly steeper than the shallow body shape (table 4, figure 5(A)). The slope for the deep body shape was not significantly different from either shape (table 4). Overall, pulse duration had a significant positive effect on the total heading change, but the slope of the interaction in the shallow body shape is not significantly different from zero, whereas the slope of the other two shapes is positive. The slopes of the interaction with deep- and medium-depth body shapes were not significantly different from one another, and both were significantly different from the slope of the shallow body shape. We expected the deeper body shapes to outperform the shallow body shape, though we did not expect the intermediate body shape to outperform the deep body shape.

The deep body shape had the lowest recoil, averaging just over three degrees, followed by the medium-depth body shape just under seven degrees, and the shallow body shape had the largest recoil with an average recoil of 22 degrees (table 3). These data are inline with our hypotheses about relative performance. Both increasing summed motor angle and pulse duration increased recoil. For the summed motor angle, the slope of the interaction with recoil was not significantly different from zero for the deep body shape (table 4, figure 5(C)), and all slopes were significantly different from one another with the shallow body slope being the steepest. For pulse duration, all interaction slopes were significantly different from one another, with the shallow body having the steepest slope, followed by the medium body, and finally the deep body (table 4, figure 5(D)).

The shallow body shape had significantly higher mean linear accelerations than the deep body shape, but the medium-depth body shape was not significantly different from either (table 3). The summed motor angle had significant, though small, negative relationships with mean linear acceleration in deep- and medium-depth body shapes (table 4, figure 6(A)). The slopes of these relationships were not significantly different. The relationship between the summed motor angle and mean linear acceleration in pulses was significantly positive in the shallow body shape, though the slope was also small (table 4, figure 6(A)).

Table 4. The interaction tests between motor angle kinematics and turn performance metrics. The slopes given are the slopes of the interaction between a given motor kinematic variable, turn performance metric, and body shape; i.e. the slope of the regression line for each body shape between two variables of interest. The significance values indicate whether the slope of the interaction between body shape and the kinematic variables is significantly different from zero. Different letters indicate significant differences between the slopes of the interactions with different body shapes.

	MOTOR KINEMATIC VARIABLE	BODY SHAPE	INTERACTION SLOPE	STD ERR	T RATIO	PROB>|T|	PAIRWISE
TOTAL HEADING CHANGE (DEG)	Summed Motor Angle (deg)	Deep	0.50	0.03	16.51	**<0.0001**	AB
		Medium	0.56	0.03	16.08	**<0.0001**	A
		Shallow	0.37	0.03	11.54	**<0.0001**	B
	Pulse Duration (sec)	Deep	10.96	1.19	9.21	**<0.0001**	A
		Medium	6.91	0.97	7.11	**<0.0001**	A
		Shallow	-0.21	1.13	-0.18	0.85	B
RECOIL (DEG)	Summed Motor Angle (deg)	Deep	0.03	0.02	1.48	0.14	A
		Medium	0.12	0.02	5.36	**<0.0001**	B
		Shallow	0.20	0.02	9.82	**<0.0001**	C
	Pulse Duration (sec)	Deep	2.47	0.76	3.25	0.001	A
		Medium	5.84	0.62	9.41	**<0.0001**	B
		Shallow	18.32	0.72	25.46	**<0.0001**	C
MEAN LINEAR ACCELERATION	Summed Motor Angle (deg)	Deep	-0.0004	0.0004	-0.97	0.33	A
		Medium	-0.001	0.0004	-1.74	0.08	A
		Shallow	0.001	0.0004	3.56	**0.0004**	B
	Pulse Duration (sec)	Deep	-0.10	0.01	-6.81	**<0.0001**	A
		Medium	-0.09	0.01	-7.91	**<0.0001**	A
		Shallow	-0.27	0.01	-19.41	**<0.0001**	B
MAXIMUM CENTRIPETAL ACCELERATION	Summed Motor Angle (deg)	Deep	0.006	0.0005	12.61	**<0.0001**	A
		Medium	0.007	0.0006	11.06	**<0.0001**	A
		Shallow	0.004	0.0005	7.08	**<0.0001**	B
	Pulse Duration (sec)	Deep	-0.27	0.02	-13.14	**<0.0001**	A
		Medium	-0.34	0.02	-20.72	**<0.0001**	B
		Shallow	-0.25	0.02	-13.08	**<0.0001**	A
MEAN LINEAR FORCE	Summed Motor Angle (deg)	Deep	-0.0007	0.0007	-1.04	0.30	A
		Medium	-0.001	0.0008	-1.30	0.20	A
		Shallow	0.003	0.0007	3.79	**0.0002**	B
	Pulse Duration (sec)	Deep	-0.19	0.03	-7.26	**<0.0001**	A
		Medium	-0.13	0.02	-5.92	**<0.0001**	B
		Shallow	-0.52	0.03	-20.67	**<0.0001**	A
MAXIMUM CENTRIPETAL FORCE	Summed Motor Angle (deg)	Deep	0.003	0.0002	12.61	**<0.0001**	A
		Medium	0.003	0.0003	11.06	**<0.0001**	A
		Shallow	0.002	0.0003	7.08	**<0.0001**	B
	Pulse Duration (sec)	Deep	-0.13	0.01	-13.14	**<0.0001**	A
		Medium	-0.16	0.008	-20.72	**<0.0001**	B
		Shallow	-0.12	0.009	-13.08	**<0.0001**	A

Pulse duration had significant negative effects on mean linear acceleration across body shapes (table 4, figure 6(B)). The slopes of deep and medium shapes were not significantly different, and both slopes were significantly smaller than the slope for the shallow body shape (table 4, figure 6(B)).

The medium-depth body shape had the highest centripetal accelerations, followed by the deep body shape and then the shallow body shape, and all pairs were significantly different (table 3). We expected the deepest body shape to outperform the intermediate body shape, followed finally by the shallow body shape. The summed motor angle had a positive effect on maximum centripetal acceleration (table 4 figure 6(C)). Pulse duration had a significantly negative effect on maximum centripetal acceleration across all shapes (table 4, figure 6(C)). The deep and shallow shapes had interaction slopes that did not significantly differ, whereas the medium-depth body shape had a slope significantly steeper than the other shapes (table 4, figure 6(D)). In contrast, the deep body shape had the highest centripetal forces, followed by the medium depth and shallow body shapes (table 4, figures 7(C) and (D)). These data match our expectations regarding the relative performance of each body shape. The relationships between control variables for the forces are the same as the accelerations (figures 7(C) and (D)).

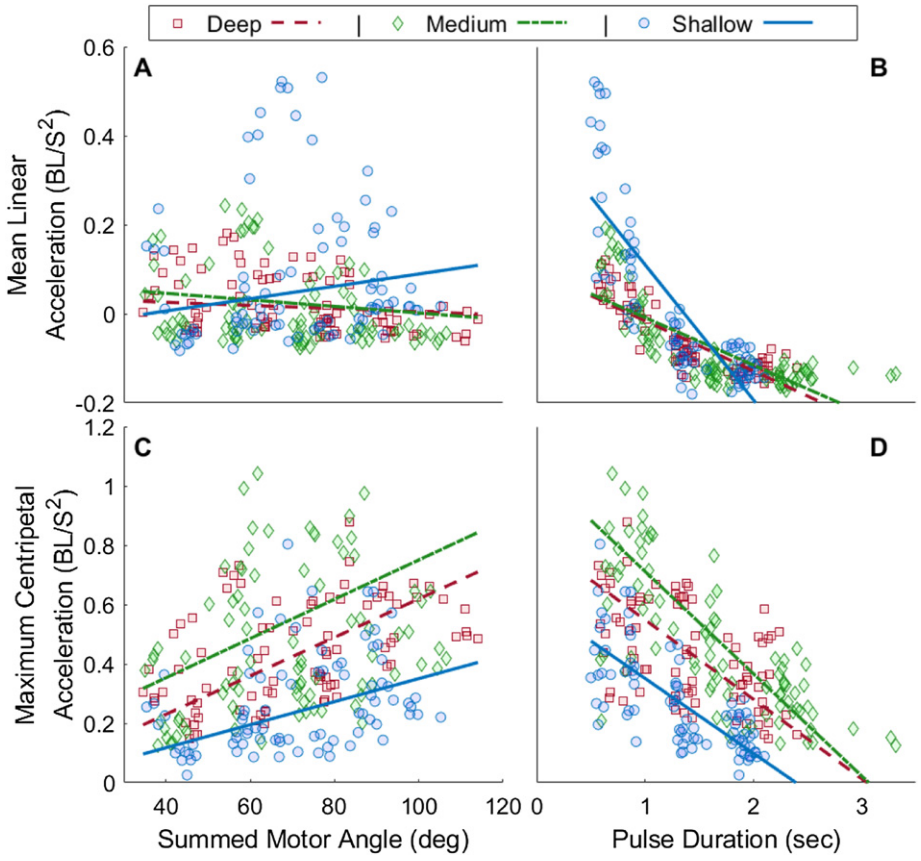

Figure 6. Linear models between measured motor kinematics and whole-body accelerations in the three robotic models. Panes (A) and (B) show the relationships between the measured control variables and linear acceleration. Panes (C) and (D) show the relationships between the measured motor control variables and centripetal acceleration.

5. Discussion

Although we found significant statistical differences between the species in terms of turn performance, we cannot make any claims about body depth's functional role in fish maneuverability as we only tested two species. We included these species in our experiment to provide biological context for our robotic model. We found that different body shapes of a robot using the same motors and commanded kinematics show substantial and significant differences in maneuverability, as predicted by Webb (1983). Robotic models are limited in their absolute performance and complexity but allow us to isolate a single variable, body depth, and keep all other shape and control variables the same. In this way we can take a much more focused approach to understand how body depth effects the function of the system. That said, there are important observations in both experiments that inform us about the nature of routine maneuvers in fish overall.

5.1. Live fish

It is impossible to draw broad conclusions about functional morphology from a comparison of two species (Garland and Adolph 1994; Lauder 1996) due to confounding variables, including behavior, motivation, and various muscle characteristics (including percent muscle mass, muscle architecture, and contractile properties). Despite the significant statistical differences in performance between the two species, their overall performance, especially the relationships between midline kinematic variables and turn performance, were similar (figure 4). Heading change correlates positively with both body curvature and turn duration, whereas acceleration correlates positively with body curvature and negatively with turn duration. These relationships are also similar to those observed in giant danio, another body-caudal fin swimming fish (Howe and Astley 2020). Webb (1978) compared the fast start performance of seven species of fish and similarly found little to no differences in the body deformation kinematics among the species, while the differences in performance were small and depended upon body size. Webb (1978) suggests that fast start performance is an optimization between lateral projected area (including fin area), the distribution of that area, and percent muscle mass, but only compares lateral projected area between two species. The applicability of these results was limited, as later studies show that the relationship between shape and maneuverability was not so clear (Gerstner 1998; Gerstner 1999; Schrank *et al* 1999).

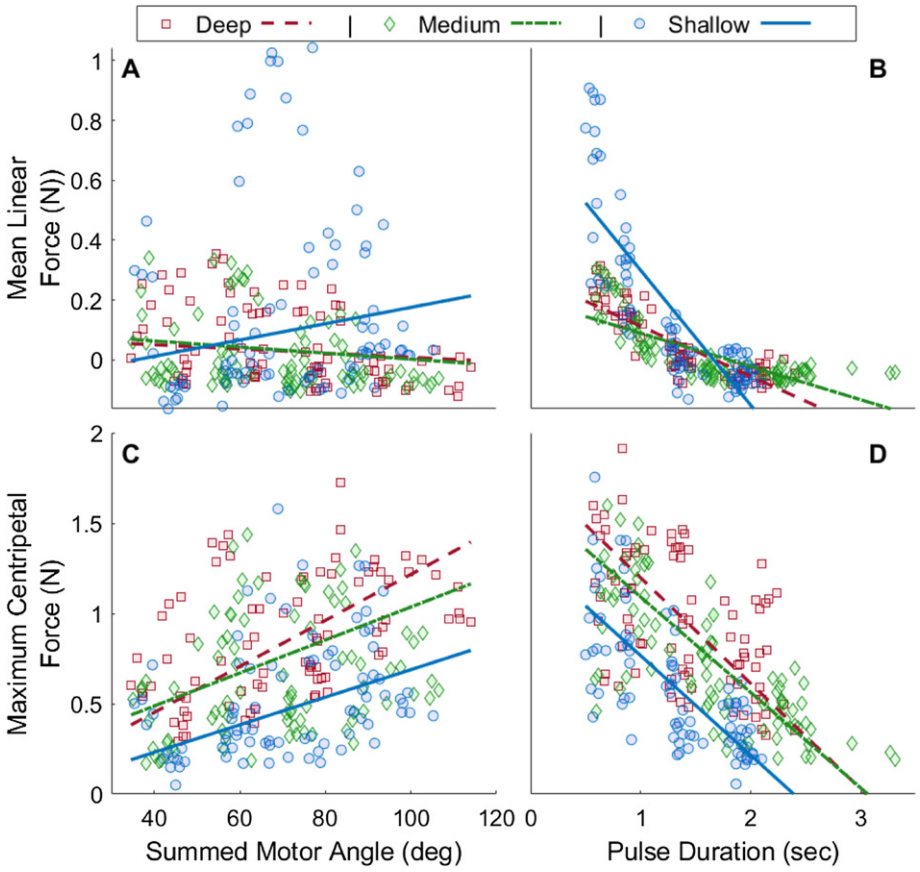

Figure 7. Linear models between measured motor kinematics and whole-body forces in the three robotic models. Panes (A) and (B) show the relationships between the measured control variables and linear forces. Panes (C) and (D) show the relationships between the measured motor control variables and centripetal forces. These forces are estimates based on the volume of each model, as discussed in the methods section.

A wider ranging study that can account for phylogeny as well as physiological and morphological differences would be helpful in understanding patterns of body shape evolution as it relates to swimming performance. Deep body shapes have evolved many times across fishes (Price *et al* 2019). Characins, cichlids, and centrarchids are all groups of primarily body caudal fin swimming species that range widely along the short/deep to elongated/shallow shape spectrum (Burns and Sidlauskas 2019; Feilich 2016; Fernando *et al* 2018). A similar deep shallow body shape spectrum exists in coral reef fishes (Claverie and Wainwright 2014), many of which use median and paired fins for most of the slow-speed swimming (Walker and Westneat 2002). Both representatives from deep bodied taxa, such as acanthurids, and shallow bodied taxa, e.g. a labrid such as *Gomphosus varius*, rely on paired fin swimming. In body caudal fin swimmers, propulsion and maneuvering are coupled; however, in median and paired fin swimmers, the median and paired fins take over the role of propulsion in slow-speed swimming, while the body is held straight (Blake 1979; George and Westneat 2019). For these species, instead of acting as a propulsor, the body may serve more as a rudder to complement the fishes ability to maneuver with its pectoral fins (Walker 2004; Walker and Westneat 2002), and the effects of body shape on maneuverability may be different for median and paired fin swimmers when compared to body caudal fin swimmers. Fish are diverse in form and behavior and it is important to continue returning to the well of live fish experiments to inform and support the design of robophysical models.

5.2. Robots

Robophysical models are excellent hypothesis testing tools to explore the effects of shape and behavior in a biological system. However, to be effective, the model must be grounded in the biological system. We include live fish turning performances in this paper to confirm that our robotic control method (from Howe *et al* 2021, based on live animal data in Howe and Astley 2020) was applicable and that fish of different body depths did not use different kinematics or control relationships during turning. Specifically, increased body curvature correlated with increased heading change, while decreased turn duration correlated with increased accelerations.

Our results showed both high qualitative and quantitative similarity in bending kinematics and the control relationships among both species of tetra

in this study, and with the giant danios tested in our prior work (Howe and Astley 2020). Knowing that the kinematics of the body deformations were very similar between species allowed us to simplify the design of the robot experiments, testing the effect of shape across a range of shared input kinematics. Had we observed significant kinematic differences between the species, we would have incorporated the interaction between shape and kinematics in the design of our robot experiment, as Borazjani and Sotiropoulos (2010) did when numerically simulating two different body shapes swimming with two different steady swimming kinematics. They show that the relationships between body shape and swimming performance change at different Reynolds numbers (Borazjani and Sotiropoulos 2010). We expect that turning kinematics may differ among species of different sizes or at different initial velocities, but this was beyond the scope of this study.

We found large and significant differences in robot performance due to body shape, while the relationships between kinematics and performance outcomes remained the same. Curvature has positive effects on heading change and acceleration (figures 5 and 6), whereas turn duration has a negative effect on acceleration and a positive effect on heading change (figures 5 and 6). Our results show that the medium-depth body shape is the best at overall maneuvering. The medium-depth shape had the highest centripetal accelerations and the highest heading changes across most motor settings (table 3, figures 6(A) and (B)). The deep body shape is very near the medium-depth body shape in terms of total heading change and outperforms the medium shape only in terms of reducing recoil. Webb (1978) identified the bluegill as having an optimal body shape for changing heading, as it had larger lateral projected areas at the head and the tail, allowing it to resist recoil as it exited the turn. Thandiackal and Lauder (2020) found that the water initially accelerated by the fish in the first phase of the turn does work on the fish's anterior body in the second phase of the turn. This work supports the body, helping the fish maintain the heading it achieved in phase one. Having a larger surface area on which the water can work will likely help reduce the recoil a fish experiences during the turn. That said, recoil does not seem to be an issue in the live fish we studied, regardless of shape (mean 95% confidence interval for all turns: 1.25–1.93°, table S1, Howe and Astley (2020), supplemental materials). This may indicate that live fish have other methods of compensating for recoil, e.g. the use of pectoral fins.

While the shallow body shape was the worst at maneuvering it was the best at linear acceleration, especially at low turn durations (figure 6). During preliminary trials, we had to adjust initial robot placement in the shallow-body robot, as it could cover the field of view before initiating the turn. The highest linear accelerations of all robot shapes occurred with the shallow robot executing short durationintermediate motor-angle turns. This is likely due to advantages in propulsive efficiency, as the shallow-body robot had a much smaller internal volume of water to accelerate, lower drag, and the tail was much larger relative to body volume. In this way the shallow-body robot resembles pike and other acceleration specialists. The shallow body depth has the highest linear accelerations at intermediate total motor angles (figure 6(A)). These high accelerations correspond to the low pulse duration turns. The high accelerations observed center around intermediate total motor angles because the shallow robot is unable to achieve the highest total motor angles (figure S2), thus increasing the number of intermediate total motor angle observations. This is likely due to the motors being unable to supply the necessary force to drive the motions to their intended angles in such a short time. The motors of the shallow body shape get closest to the ideal motor positions, with the medium and deep body depths progressively under-performing (figure S2).

In a similar vein, we found that the intermediate body depth had higher accelerations than the deepest body shape, despite the deepest body shape having significantly higher estimated centripetal force (figure 7). In this case, the intermediate body shape probably had enough lateral area to generate significant centripetal forces, but not to the point where the acceleration penalties incurred by increasing mass would diminish the effects of the forces generated by the lateral area. In this experiment we chose to keep the body width of our robots consistent across body shapes. In many cases we find that deep-bodied fish are often laterally compressed (Claverie and Wainwright 2014; Price *et al* 2019), meaning that these fish are thinner than one would expect given their body depth, allowing them to simultaneously reduce their mass and increase their lateral area. Had we controlled for body volume we might have seen that the deepest body shape generated the highest centripetal accelerations, though given the physical and mechanical constraints in the construction of the robot, this was not feasible.

There are several design choices we made in our robot for consistency and simplicity, including a forked tail shape of constant size. Tail shape is highly variable across fish and has large effects on the hydrodynamics of the system (Feilich and Lauder 2015; Van Buren *et al* 2017). To simplify the design of the robot we did not include median fins. The dorsal and anal fins are a very important part of the fish swimming system as they add, often significantly, to the lateral area of the fish, and help shape the vortices that ultimately power the turn. Some studies have investigated the effects of median fins on steady swimming in different fish (Tytell, 2006; Tytell and Lauder 2008). Simulations of fish turning that include median fins suggest that fish benefit from having erected fins early in the turn to maximize lateral projected area and

then should collapse their fins to reduce drag penalties while accelerating out of the turn (Singh and Pedley 2012), but this has not been tested in live fish or robots. Webb (1978) observed that fish initiate escape responses with erect fins, though does not mention whether those fins collapse upon exiting the turn. Our robot was also dorsoventrally symmetric and was deepest at approximately mid-length. While this is a biologically relevant model, there are other ways to distribute lateral projected area that may affect the results. Many fish including pomacentrids, chaetodontids, and others have lateral projected areas concentrated around the tail, whereas mahi mahi (*Coryphaena hippurus*) have lateral areas that are anteriorly weighted. Many species, including the black skirt tetra but especially fish from the family *Gasteropelecidae*, have ventrally weighted lateral projected areas. These traits may or may not have evolved to enhance maneuverability but will likely have hydrodynamic effects on their swimming ability. A robotic model would be able to test for these effects while controlling the other traits.

6. Conclusions

Using robotic models and live fish we clarify the effects of deepening body morphologies on fish maneuverability. Increasing body depth allows a fish to achieve tighter turns and centripetally accelerate more than the shallowest body depths, though there are diminishing returns on acceleration as the body continues to deepen. Even though the live fish did not differ in performance as hypothesized, their kinematics informed the design of our robotic experiments and confirmed the kinematic patterns observed. We were also able to gather a large sample of maneuvers that support and expand upon earlier observations on how body deformation during a turn affects the outcomes of a turn. Further study is needed to understand how other components of a fish's morphology interact with body shape to achieve maneuvers, especially the shape and placement of median fins. In this paper, we examined maneuverability in two species of fish, and the wider literature adds several dozen to that number. As more varieties of fish are examined, we will better understand the rules that govern maneuverability and locomotion more generally. Incorporating the knowledge gained from studying fish into the robotic models we build will improve the performance of those models, which will make them more useful as tools for testing biological hypotheses.

Acknowledgments

The authors thank Liann Cox and the University of Akron lifeguards for providing access to the pool and support during the experiment, and Peter Niewiarowski for advice on statistical methods.

Data availability statement

The data that support the findings of this study are openly available at the following (Howe *et al* 2021) URL/DOI: https://doi.org/10.5061/dryad.1g1jwstwj

ORCID iDs

Stephen Howe https://orcid.org/0000-0003-0436-9078
Kelly Bryant https://orcid.org/0000-0003-3129-0998
Andrew Duff https://orcid.org/0000-0002-1489-6624
Henry Astley https://orcid.org/0000-0003-0136-1433

References

Aguilar J *et al* 2016 A review on locomotion robophysics: the study of movement at the intersection of robotics, soft matter and dynamical systems *Rep. Prog. Phys.* **79** 110001
Astley H C 2016 The diversity and evolution of locomotor muscle properties in anurans *J. Exp. Biol.* **219** 3163–73
Blake R W 1979 The mechanics of labriform locomotion: I. Labriform locomotion in the angelfish (*Pterophyllum eimekei*): an analysis of the power stroke *J. Exp. Biol.* **82** 255–71
Borazjani I and Sotiropoulos F 2010 On the role of form and kinematics on the hydrodynamics of self-propelled body/caudal fin swimming *J. Exp. Biol.* **213** 89–107
Boulenger G 1895 Abstract of a report on a large collection of fishes formed by Dr. C Ternetz in Matto Grosso and Paraguay, with descriptions of new species *Proc. Zool. Soc. Lond.* **2** 523–9
Brönmark C and Miner J G 1992 Predator-induced phenotypical change in body morphology in crucian carp *Science* **258** 1348–50
Burns M D and Sidlauskas B L 2019 Ancient and contingent body shape diversification in a hyperdiverse continental fish radiation *Evolution* **73** 569–87
Claverie T and Wainwright P C 2014 A morphospace for reef fishes: elongation is the dominant axis of body shape evolution *PLoS One* **9** e112732
Costa-Pereira R, Araújo M, Paiva F and Tavares L 2016 Functional morphology of the tetra fish *Astyanax lacustris* differs between divergent habitats in the Pantanal wetlands *J. Fish Biol.* **89** 1450–8
Domenici P, Turesson H, Brodersen J and Brönmark C 2008 Predator-induced morphology enhances escape locomotion in crucian carp *Proc. R. Soc. B.* **275** 195–201
Eigenmann C H and Kennedy C H 1903 On a collection of fishes from Paraguay, with a synopsis of the American genera of cichlids *Proc. Acad. Nat. Sci. Phila.* **55** 497–537
Feilich K L 2016 Correlated evolution of body and fin morphology in the cichlid fishes *Evolution* **70** 2247–67
Feilich K L and Lauder G V 2015 Passive mechanical models of fish caudal fins: effects of shape and stiffness on self-propulsion *Bioinsp. Biomim.* **10** 036002
Felsenstein J 1985 Phylogenies and the comparative method *Am. Nat.* **125** 1–15
Fernando A V, Hecke K B and Eggleton M A 2018 Length, body depth, and gape relationships and inference on piscivory among common North American centrarchids *Southeast. Nat.* **17** 309–26
Fleuren M, van Leeuwen J L, Quicazan-Rubio E M, Pieters R P M, Pollux B J A and Voesenek C J 2018 Three-dimensional analysis of the fast-start escape response of the least killifish, *Heterandria formosa J. Exp. Biol.* **221** jeb168609

Foster K, Bower L and Piller K 2015 Getting in shape: habitat-based morphological divergence for two sympatric fishes *Biol. J. Linn. Soc.* **114** 152–62

Franssen N R, Stewart L K and Schaefer J F 2013 Morphological divergence and flow-induced phenotypic plasticity in a native fish from anthropogenically altered stream habitats *Ecol. Evol.* **3** 4648–57

Garland T Jr and Adolph S C 1994 Why not to do two-species comparative studies: limitations on inferring adaptation *Physiol. Zool.* **67** 797–828

George A B and Westneat M W 2019 Functional morphology of endurance swimming performance and gait transition strategies in balistoid fishes *J. Exp. Biol.* **222** jeb194704

Gerry S P, Belden J, Bisaccia M, George K, Mahoney T and Ellerby D J 2016 Scaling of the fast-start escape response of juvenile bluegills *Zoology* **119** 518–25

Gerstner C L 1998 The function of a deep body morphology in coral reef fishes: enhanced maneuverability or protection from gape-limited predators? *PhD Dissertation* University of Michigan

Gerstner C L 1999 Maneuverability of four species of coral-reef fish that differ in body and pectoral-fin morphology *Can. J. Zool.* **77** 1102–10

Haas T C, Heins D C and Blum M J 2015 Predictors of body shape among populations of a stream fish (*Cyprinella venusta*, cypriniformes: cyprinidae) *Biol. J. Linn. Soc.* **115** 842–58

Howe S P and Astley H C 2020 The control of routine fish maneuvers: connecting midline kinematics to turn outcomes *J. Exp. Zool.* A **333** 579–94

Howe S P, Duff A R and Astley H C 2021 Comparing the turn performance of different motor control schemes in multilink fish-inspired robots *Bioinsp. Biomim.* **16** 036010

Howe S, Bryant K, Duff S and Astley H 2021 Testing the effects of body depth on fish maneuverability via robophysical models *Bioinspir. Biomim.* https://doi.org/10.5061/dryad.1g1jwstwj

Istead A E, Yavno S and Fox M G 2015 Morphological change and phenotypic plasticity in response to water velocity in three species of *Centrarchidae Can. J. Zool.* **93** 879–88

Jayne B C and Lauder G V 1993 Red and white muscle activity and kinematics of the escape response of the bluegill sunfish during swimming *J. Comp. Physiol.* A **173** 495–508

Langerhans R B 2009 Trade-off between steady and unsteady swimming underlies predator-driven divergence in *Gambusia affinis J. Evol. Biol.* **22** 1057–75

Lauder G V 1996 The arguement from design *Adaptation* ed ed M R Rose and G V Lauder (New York: Academic) ch 2

Moody E K and Lozano-Vilano M L 2018 Predation drives morphological convergence in the *Gambusia panuco* species group among lotic and lentic habitats *J. Evol. Biol.* **31** 491–501

Nilsson P A, Brönmark C and Pettersson L B 1995 Benefits of a predator-induced morphology in crucian carp *Oecologia* **104** 291–6

Price S, Friedman S, Corn K, Martinez C, Larouche O and Wainwright P 2019 Building a body shape morphospace of teleostean fishes *Integr. Comp. Biol.* **59** 716–30

Rubio-Gracia F, García-Berthou E, Latorre D, Moreno-Amich R, Srean P, Luo Y and Vila-Gispert A 2020 Differences in swimming performance and energetic costs between an endangered native toothcarp (*Aphanius iberus*) and an invasive mosquitofish (*Gambusia holbrooki*) *Ecol. Freshw. Fish* **29** 230–40

Schrank A J, Webb P W and Mayberry S 1999 How do body and paired-fin positions affect the ability of three teleost fishes to maneuver around bends? *Can. J. Zool.* **77** 203–10

Shelton R M, Thornycroft P J and Lauder G V 2014 Undulatory locomotion of flexible foils as biomimetic models for understanding fish propulsion *J. Exp. Biol.* **217** 2110–20

Singh K and Pedley T J 2012 Modelling lateral manoeuvres in fish *J. Fluid Mech.* **697** 1–34

Svozil D P, Baumgartner L J, Fulton C J, Kopf R K and Watts R J 2020 Morphological predictors of swimming speed performance in river and reservoir populations of Australian smelt *Retropinna semoni Journal of Fish Biology* **97** 1632–43

Tangorra J L, Lauder G V, Hunter I W, Mittal R, Madden P G A and Bozkurttas M 2010 The effect of fin ray flexural rigidity on the propulsive forces generated by a biorobotic fish pectoral fin *J. Exp. Biol.* **213** 4043–54

Thandiackal R and Lauder G V 2020 How zebrafish turn: analysis of pressure force dynamics and mechanical work *J. Exp. Biol.* **223** jeb223230

Tytell E D 2006 Median fin function in bluegill sunfish (*Lepomis macrochirus*): streamwise vortex structure during steady swimming *J. Exp. Biol.* **209** 1516–34

Tytell E D and Lauder G V 2008 Hydrodynamics of the escape response in bluegill sunfish, *Lepomis macrochirus J. Exp. Biol.* **211** 3359–69

Van Buren T, Floryan D, Brunner D, Senturk U and Smits A J 2017 Impact of trailing edge shape on the wake and propulsive performance of pitching panels *Phys. Rev. Fluids* **2** 059901

Wahl D H and Stein R A 1988 Selective predation by three esocids: the role of prey behavior and morphology *Trans. Am. Fish. Soc.* **117** 142–51

Walker J A 2004 Kinematics and performance of maneuvering control surfaces in teleost fishes *IEEE J. Ocean. Eng.* **29** 572–84

Walker J A and Westneat M W 2002 Performance limits of labriform propulsion and correlates with fin shape and motion *J. Exp. Biol.* **205** 177–87

Webb P W 1978 Fast-start performance and body form in seven species of teleost fish *J. Exp. Biol.* **74** 211–26

Webb P W 1983 Speed, acceleration and manoeuvrability of two teleost fishes *J. Exp. Biol.* **102** 115–22

Westneat M, Hale M, McHenry M and Long J 1998 Mechanics of the fast-start: muscle function and the role of intramuscular pressure in the escape behavior of *Amia calva* and *Polypterus palmas J. Exp. Biol.* **201** 3041–55

Wolf Z, Jusufi A, Vogt D M and Lauder G V 2020 Fish-like aquatic propulsion studied using a pneumatically-actuated soft-robotic model *Bioinsp. Biomim.* **15** 046008

Yan G-J, He X-K, Cao Z-D and Fu S-J 2013 An interspecific comparison between morphology and swimming performance in cyprinids *J. Evol. Biol.* **26** 1802–15